Effect of Positively Charged Lipids (DOTAP) on the Insertion of CNT into Liposomes and Separation Performance of Tfn Membranes

Jianjun Zhao , Junqing Sun , Kefeng Zhang * , Shan Wang , Wande Ding * , Zhengping Li

Posted Date: 3 January 2024

doi: 10.20944/preprints202401.0120.v1

Keywords: thin-film nanocomposite; carbon nanotube; liposomes; DOTAP; desalination

Article

Effect of Positively Charged Lipids (DOTAP) on the Insertion of CNT into Liposomes and Separation Performance of TFN Membranes

Jianjun Zhao [1], Junqing Sun [1], Kefeng Zhang [1,*], Shan Wang [1], Wande Ding [1,2,*] and Zhenping Li [3]

[1] School of Municipal and Environmental Engineering, Shandong Jianzhu University, Jinan, 250101, China
[2] Shandong Shuifa Environmental Technology Co., Ltd, Jining, 272000, China
[3] State Key Laboratory of Biobased Material and Green Papermaking, Qilu University of Technology (Shandong Academy of Sciences), Jinan, 250353, China
* Correspondence: kfz@sdjzu.edu.cn (K.Z.); dingwande18@sdjzu.edu.cn (W.D.)

Abstract: Liposome vesicle is an ideal carrier for carbon nanotube (CNT) to serve as the water channel that allows the fast transport of water molecules, and thus enhancing the membrane permeability. However, low quantity of the inserted CNT in the liposome vesicle is an important factor that limited further improvement of the membrane flux. In present study, positively charged lipids (2,3-dioleoyloxy-propyl)-trimethylammonium-chloride (DOTAP) was introduced to the 1,2-dioleoyl-sn-glycero-3-phosphoethanolamineon (DOPE) liposome vesicles to tailor the vesicle charge, so as to evaluate the effect of positively charged DOTAP on the insertion of CNT into liposomes and separation performance of thin-film nanocomposite (TFN) membranes. The results showed that addition of DOTAP induced more quantity of CNT inserted into the liposome vesicles, since the shrinkage rate (*k*) and permeability (*Pf*) of liposome vesicles present obvious increase with increased content of DOTAP in the liposome vesicles. Besides, it contributed to 252.3% higher water flux for TFN membranes containing DOPE/DOTAP$_{2:1}$-CNT liposomes (the mass ratio between DOPE and DOTAP was 2:1) than TFC membranes. More important, it presented 106.7% higher water flux for TFN membranes containing DOPE/DOTAP$_{4:1}$-CNT liposomes (the mass ratio between DOPE and DOTAP was 4:1), which was originated from the more water channels that the CNT provided in the liposome vesicles. In all, positively charged DOTAP effectively tailored the vesicle charge, which provided a better carrier for the insertion of more quantity of CNT, and contributed to higher permeability of TFN membranes.

Keywords: thin-film nanocomposite; carbon nanotube; liposomes; DOTAP; desalination

1. Introduction

With the continuous increase of population and the serious water pollution, the shortage of fresh water is gradually becoming an important problem that need to be addressed urgently[1,2]. Nowadays, reverse osmosis (RO) technology has developed to be one of the main methods to solve the freshwater crisis because of its great separation efficiency and low energy consumption, which has showed great application value in the fields of seawater desalination, brackish water desalination and wastewater reuse[3]. As the core of RO technology, the properties of RO membrane directly affect the separation efficiency and the quality of water production, and development of high-performance RO membrane has been the research hotspot in the membrane field at home and abroad. Polyamide composite membranes (PA-TFC) prepared by interfacial polymerization method is now occupying the dominant position in the RO membrane market[4,5]. However, due to the mutual restriction-"trade-off" effect (balance between water flux and salt rejection), TFC membranes always show low permeability but high rejection of salt ions[6,7].

In 2007, Hoek et al. first proposed the concept of "thin-film nanocomposite membrane (TFN)", which gradually developed into one of the effective means to break through the "trade-off" effect[8]. On the one hand, incorporation of nanomaterials in the polyamide layer (PA) could provide low-

resistance water channel that promotes the permeation of water molecules. On the other hand, nanomaterials could induce the improvement of surface physical and chemical properties. Among the various nanomaterials, carbon nanotubes (CNT) are deemed as the most valuable nanofillers in overcoming the inherent limitation of "trade-off" effect due to the physical and chemical properties, especially for its ultra-fast rate for water transportation through the inner wall[9,10]. Currently, physical blending is the most commonly used method in preparing CNT-based TFN RO membranes, in which CNT is added in aqueous phase or organic phase. Johnson et al. incorporated zwitterion modified CNT in the PA layer, and the membrane flux increased from 11 L/m²·h for TFC membranes to 48 L/m²·h for TFN membranes with unchanged salt rejection[11]. Besides, Zhang et al. first graft OH group to the surface of CNT and then was added in aqueous phase to prepare the TFN membrane. Resultantly, two times higher water flux obtained compared to TFC membrane[12]. Up to now, several research groups have proved that CNT was indeed played an important role in enhancing the membrane permeability and the antifouling capacity[13–15].

In 2023, our group first reported the effect of CNT nanochannel on the permeability of TFN membranes, in which COOH-SWCNT was inserted in the 1,2-dioleoyl-sn-glycerol-3-phosphocholine (DOPC) liposomes and then embedded in the PA layer. The resultant membrane showed 71.4 % enhancement of water flux compared to TFC membranes, but merely 25.6 % was induced by the CNT nanochannel[16]. The relative lower contribution of CNT nanochannel was mainly caused by the low content of the inserted CNT. Therefore, increase the content of the inserted CNT in the liposomes is important to further enhance the membrane flux. Inspired by the aquaporin (AQP)-based biomimetic membranes, liposome charge is an important factor in influencing the quantity of the inserted water channel in the liposomes[17]. For instance, by introducing positively charged (2,3-dioleoxy-propyl) trimethylammonium chloride (DOTAP) phospholipid molecules into the neutral phospholipid molecules (DOPE), Wang et al. found that the phospholipid vesicles penetration rate increased from 1561.5 μm·s⁻¹ to 2537.7 μm·s⁻¹, which was due to the regulation of the electrical properties of phospholipid vesicles, thereby improving the loading ratio of water channels[18]. Whether the positively charged DOTAP could promote the insertion of more CNT in the liposomes and further contribute to higher water flux of the TFN membranes, that deserves further comprehensive study.

In current study, four types of liposomes (DOPE/DOTAP$_{4:1}$, DOPE/DOTAP$_{2:1}$ DOPE/DOTAP$_{4:1}$-CNT and DOPE/DOTAP$_{2:1}$-CNT liposomes) were synthesized and then incorporated in the selective layer to fabricate TFN membranes. Both the liposomes and TFN membranes were characterized by several advanced techniques including Stop-Flow, XPS, SEM, etc., to determine the effect of positively charged DOTAP on the insertion of CNT into liposomes and micro-structure of PA layer. What's more, the influence of positively charged DOTAP on the separation and antifouling performance was also evaluated. In all, the current work was in an attempt to increase the quantity of inserted CNT in the liposomes and contribute to higher water flux of TFN membranes.

2. Experimental

2.1. Preparation of liposomes and CNT-liposomes

Liposomes and CNT-liposomes were synthesized through a combined rehydration and extrusion method according to the previous work. Of note, prior to the fabrication of CNT-liposomes, length shorten of CNT was needed. Detailed procedure can be found in Text S1 and Text S2. Finally, DOPE/DOTAP$_{4:1}$, DOPE/DOTAP$_{2:1}$ DOPE/DOTAP$_{4:1}$-CNT and DOPE/DOTAP$_{2:1}$-CNT liposomes were prepared with the final concentration about 1.0 mg/mL.

2.2. Fabrication of TFC and TFN membranes

TFC and TFN membranes were prepared through traditional IP reaction. Briefly, the top surface of the ultrafiltration membrane was first contacted with aqueous solution (containing 2 w/v% MPD and 0.1 w/v% SDS) for 2 min. After removing the aqueous solution, the top surface was contacted with organic phase (containing 0.1 w/v% TMC/n-hexane) for another 1 min. Then, the resultant TFC membranes were heat-treated in an oven for 5 min at 80 °C to complete the IP reaction. For TFN

 doi:10.20944/preprints202401.0120.v1

membranes, various types of liposomes under different loading concentration (ranging from 0.1 mg/mL to 1.0 mg/mL) was mixed with aqueous solution, followed by the same preparation procedure as TFC membranes. To distinguish the different TFN membranes, the membrane containing DOPE/DOTAP$_{4:1}$ was denoted as TFN$_{4:1}$-x, the membrane containing DOPE/DOTAP$_{2:1}$ was denoted as TFN$_{2:1}$-x, the membrane containing DOPE/DOTAP$_{4:1}$-CNT was denoted as TFN$_{4:1}$-CNT-x and the membrane containing DOPE/DOTAP$_{2:1}$-CNT was denoted as TFN$_{2:1}$-CNT-x, where x represents the mass concentration (mg/mL) of liposomes or CNT-liposomes.

2.3. Membrane separation performance

Water flux and salt rejection of all the membranes were determine by a cycle cross-flow filtration setup (FlowMen-0021-HP, Figure S1). The effective membrane area was 24 cm^2 and 2000 ppm NaCl was used as the feed solution. The membrane should be pre-compressed under 18 bar until a stable permeance achieved. Then, the operation pressure was adjusted to 16 bar to determine the water flux (J, $L/m^2 \cdot h$) and salt rejection (R, %), which were calculated by the following equations[19,20]:

$$J = \frac{\Delta V}{S \cdot \Delta t} \quad (1)$$

$$R = 1 - \frac{C_2}{C_1} \quad (2)$$

where ΔV (L), S (m^2), Δt (h), C_2 (g/L), C_1 (g/L) represent the permeate volume, the effective membrane area, the operation time, and the permeate and feed concentration, respectively. Other characterization method can be found in Text S3.

2.4. Antifouling performance

The fouling test contained two cycles, and each cycle consisted fouling-rinsing process. In the fouling process, 500 ppm HA and 2000 ppm NaCl was first used as the feed solution to conducted the fouling filtration for 9 h. After fouling process, the membrane underwent 2 h rinsing with DI water under high-flow rate without pressure input. Finally, the cleaned membrane was retested to obtain the recovered flux. The flux recovery rate (FRR, %), and all antifouling parameters were calculated by the following equations[3,16]:

$$FRR = \frac{J_1}{J_0} * 100\% \quad (3)$$

$$R_t = \frac{TMP}{\mu J} = R_m + R_r + R_{ir} \quad (4)$$

$$R_m = \frac{TMP}{\mu J_0} \quad (5)$$

$$R_t = \frac{TMP}{\mu J_2} \quad (6)$$

$$R_r = \frac{TMP}{\mu J_2} - \frac{TMP}{\mu J_1} \quad (7)$$

$$R_{ir} = R_t - R_m - R_r \quad (8)$$

where J_0 ($L/m^2 \cdot h$) is the initial flux, J_1 ($L/m^2 \cdot h$) is the permeate flux at the end of fouling process, J_2 ($L/m^2 \cdot h$) is the recovered water flux after rinsing, R_t (m^{-1}) is the total membrane fouling resistance, R_m (m^{-1}) is the intrinsic membrane resistance, R_r (m^{-1}) is the hydraulic reversible resistance, R_{ir} (m^{-1}) is the irreversible fouling resistance, TMP (Pa) is the trans-membrane pressure and μ ($Pa \cdot s$) is the dynamic viscosity for the feed water.

3. Result and discussion

3.1. Characterization of liposomes

The FTIR spectra of different liposomes were shown in Figure 1a. Both DOPE/DOTAP liposomes and DOPE/DOTAP-CNT liposomes exhibited typical absorption peaks of lipids. In detail, the peaks at 1062 cm^{-1} belongs to the CN stretching of the primary amine. The peaks at 1228 cm^{-1} and 1372 cm^{-1} were assigned to the P=O stretching of phosphates provided by the DOPE lipid[21]. Besides, a major

Preprints (www.preprints.org) | NOT PEER-REVIEWED | Posted: 3 January 2024 doi:10.20944/preprints202401.0120.v1

peak at 1641 cm^{-1} was originated from the NH bending and abundance of DOTAP lipid in the DOPE-DOTAP[22]. After insertion of CNT, two new peaks appeared at 1512 cm^{-1} and 1249 cm^{-1}, which were attributed to the C=C vibration in the backbone of the carbon nanotube and C–C vibration mode of CNT. It was noticed that insertion of CNT induced red/blue shift of the absorption peaks of the lipids, indicating the complex interactions between lipids and CNT[23,24]. Raman spectra of DOPE/DOTAP liposomes and DOPE/DOTAP-CNT liposomes were displayed in Figure 1b,c. The characteristic signals of G-band and D-band for CNT were observed clearly at 1590 cm^{-1} and 1340 cm^{-1}, and the signal intensity of G-band and D-band for DOPE/$DOTAP_{2:1}$-CNT liposomes were higher than that for DOPE/$DOTAP_{4:1}$-CNT liposomes, which suggested that more CNT nanotubes were combined with DOPE/$DOTAP_{2:1}$ liposome[25]. Besides, Near Infrared (NIR) absorbance (Figure 1d) in the 980 nm region corresponding to the S_{22} transitions in CNT further demonstrated that positively charged lipids (DOTAP) increased the quantity of CNT inserted into the liposomes, since DOPE/$DOTAP_{2:1}$-CNT exhibited higher signal intensity[26,27].

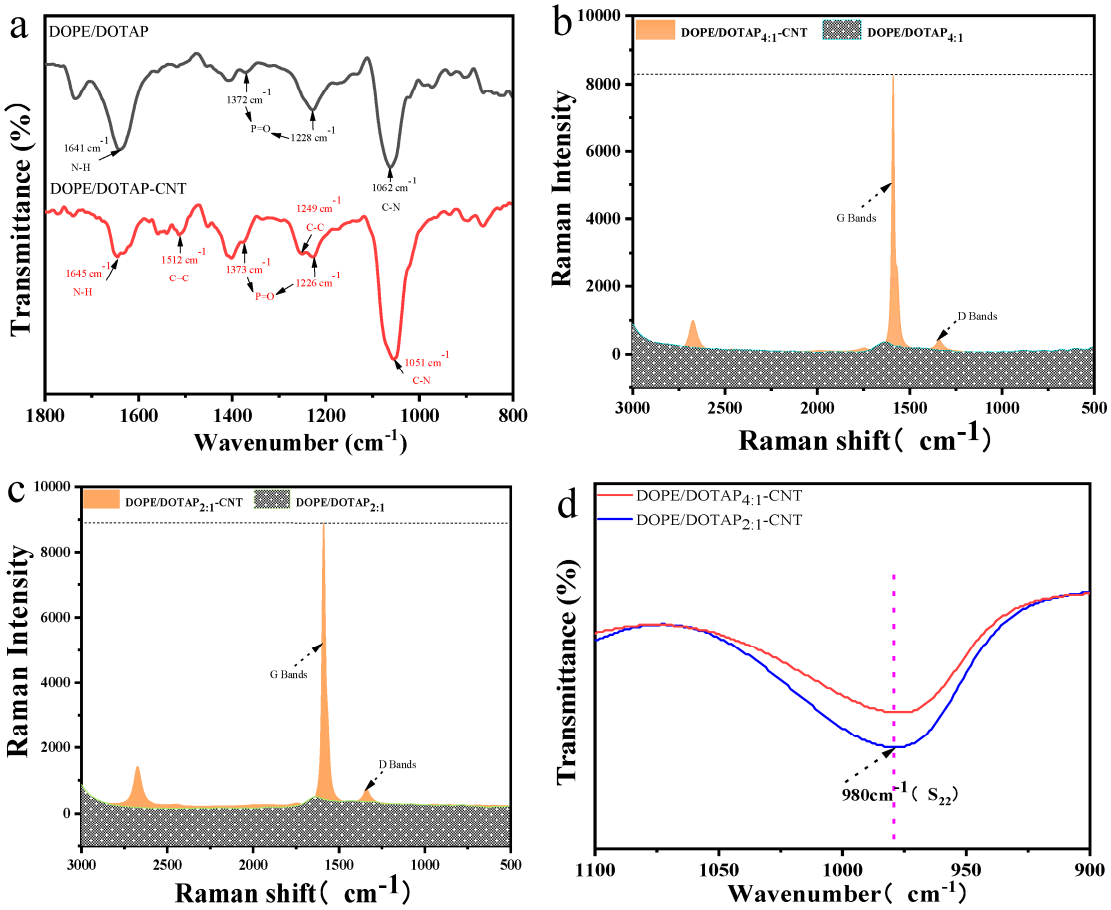

Figure 1. Physical and chemical properties of liposomes and CNT-liposomes.

Table 1 summarized the physical properties of four different liposomes. For DOPE/$DOTAP_{4:1}$ liposome, the average size was 73.66 nm with a low PDI value about 0.124 and the morphology characterized by TEM can be found in Figure S2. Besides, it showed slight positive charge about 10.60 mV due to the incorporation of the positively charged DOTAP[18]. When increasing the amount of DOTAP to the mass ratio of DOPE/DOTAP to 2:1 (DOPE/$DOTAP_{2:1}$), the average size and PDI value showed tiny changes while the zeta potential increased obviously to 25.03 mV, which was believed to be benefit for the insertion of more CNT into liposomes due to the stronger electrostatic interaction[28]. Compared to DOPE/DOTAP pure liposomes, insertion of CNT induced the increase of the average size of the DOPE/DOTAP-CNT liposomes (93.16 nm for DOPE/$DOTAP_{4:1}$-CNT and 100.70 nm for DOPE/$DOTAP_{2:1}$-CNT). Meanwhile, the PDI value also showed apparent increase, suggesting that DOPE/DOTAP-CNT liposomes were less uniform than DOPE/DOTAP pure

 doi:10.20944/preprints202401.0120.v1

liposomes[16]. Of note, DOPE/DOTAP$_{2:1}$-CNT liposomes exhibited more decline extent of zeta potential from 25.03 mV to -2.45 mV than DOPE/DOTAP$_{4:1}$-CNT liposomes from 10.60 mV to -7.13 mV due to the more negatively charged CNT inserted in the liposomes.

Table 1. Physical properties of different liposomes.

Liposomes type	Average size (nm)	PDI	Zeta potential (mV)	k (s^{-1})	Pf (μm/s)
DOPE/DOTAP$_{4:1}$	73.66	0.124	10.60	21.48	50.52
DOPE/DOTAP$_{4:1}$-CNT	93.16	0.228	-7.13	206.17	616.21
DOPE/DOTAP$_{2:1}$	77.18	0.131	25.03	23.47	57.84
DOPE/DOTAP$_{2:1}$-CNT	100.70	0.237	-2.45	221.73	712.91

What's more, Table 1 also displayed the shrinkage rate (k) and the water permeability (Pf) of DOPE/DOTAP and DOPE/DOTAP-CNT liposomes and the relevant Figure was shown in Figure S3. As observed, DOPE/DOTAP pure liposomes showed small k values (21.48 s^{-1} for DOPE/DOTAP$_{4:1}$ liposome and 23.47 s^{-1} for DOPE/DOTAP$_{2:1}$ liposomes) and low water permeability (50.52 μm·s^{-1} for DOPE/DOTAP$_{4:1}$ liposome and 57.84 μm·s^{-1} for DOPE/DOTAP$_{2:1}$ liposomes). However, it was interesting to find that pure liposomes were not thoroughly impermeable and addition of DOTAP induced slight increase in the permeability of liposomes[29]. On the contrary, DOPE/DOTAP$_{4:1}$-CNT liposomes presented sharp increment with higher k value (50.52 s^{-1}) within a short period, accompanied by twelve-times higher permeability (616.21 μm·s^{-1}), which resulted from the fast transport of water molecules through the inner wall of CNT. More important, higher content of DOTAP in the mixed liposomes contributed to higher permeability (712.91 μm·s^{-1}), which further proved the positive effect of DOTAP in the insertion of CNT into liposomes.

3.2. Characterization of TFC and TFN membranes

Surface functional groups of TFC and TFN membranes

FTIR spectra of TFC and TFN membranes were displayed in Figure 1a. All the TFC and TFN membranes exhibited typical absorption peaks of polyamide membranes. In detail, the peaks at 1662 cm^{-1} and 1607 cm^{-1} were originated from the C=O stretching vibrations (amide I), and the peak at 1542 cm^{-1} was assigned to the N–H and C–N stretching vibrations (amide II), respectively. In addition, the peak at 1449 cm^{-1} was caused by the C=O stretching and O–H bending of carboxyl group, which was formed by the transformation of the residual acyl chloride group[30–32]. Compared to TFC membranes, all the TFN membranes showed new peak at 1041 cm^{-1}, which was caused by the P–O–C group of phosphates provided by the DOPE lipid and proved the successful incorporation of liposomes[17,33]. Figure 2b showed the XRD pattern of TFC and TFN membranes. It was found that no obvious difference between TFC and TFN membranes since the liposomes possessed no typical crystal structure and the content of CNT in the liposomes was tiny.

Preprints (www.preprints.org) | NOT PEER-REVIEWED | Posted: 3 January 2024 doi:10.20944/preprints202401.0120.v1

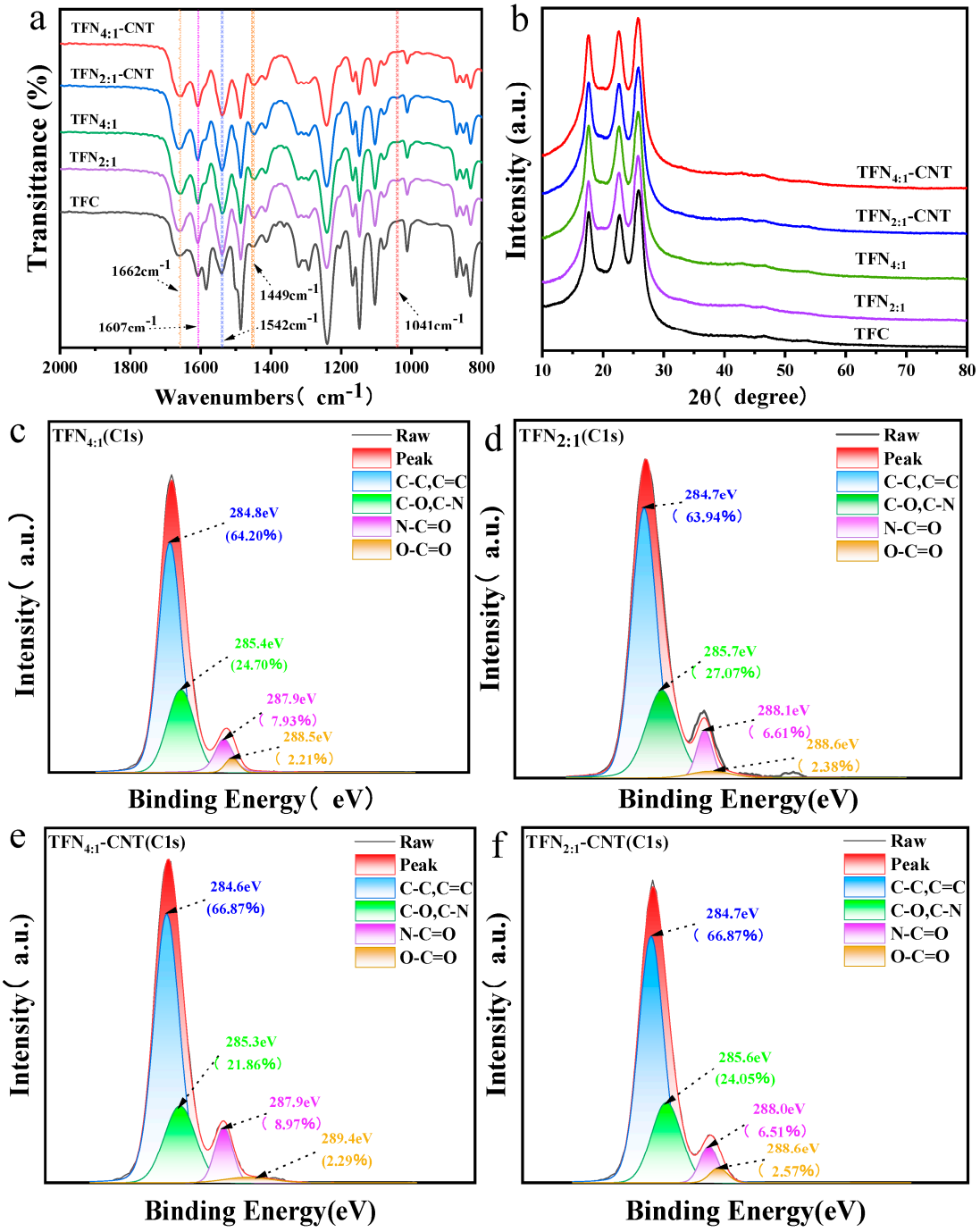

Figure 2. Surface functional groups of TFC and TFN membranes.

Figure 2c–f displayed the surface functional groups through fitting the C1s peak characterized by XPS. As obtained, the C1s can be deconvoluted into C–C/C=C (284.6 eV~284.8 eV), C-O/C-N (285.3 eV~285.7 eV), N-C=O (287.9 eV~288.1 eV) and O-C=O (288.5 eV~289.4 eV), which were typical functional groups of PA layer[34,35]. It should be emphasized that the content of surface COOH that transformed from the residual acyl chloride group was essential in influencing the membrane hydrophilicity and membrane permeability. As analyzed by the XPS results, compared to $TFN_{4:1}$ and $TFN_{4:1}$-CNT membranes, $TFN_{2:1}$ and $TFN_{2:1}$-CNT membranes presented slightly higher content of COOH on the membrane surface, which was mostly caused by the more positively charged DOTAP that interfered the IP process. Of note, insertion of CNT induced further slight increase of content of COOH on the membrane surface (2.38% for $TFN_{2:1}$ membrane to 2.57% for $TFN_{2:1}$-CNT membrane).

 doi:10.20944/preprints202401.0120.v1

Table 2 summarized the element content, $R_{O/N}$ and *D* of four TFN membranes. Generally, the lower *D* value was, the loosener structure of PA layer formed, which may contribute to the enhancement of the water permeation[3]. As obtained from Table 2, the cross-linking degree was negatively correlated to the content of COOH and DOTAP played a significant role in decreasing the cross-linking degree. In detail, the cross-linking degree of $TFN_{4:1}$ and $TFN_{4:1}$-CNT membranes were above 70%, which implied a relative dense PA layer formed on the membrane surface. Besides, the influence of CNT on the cross-linking degree can be roughly ignored. When increase the content of DOTAP in the liposomes to 2:1, it was seen that the cross-linking degree of $TFN_{2:1}$ and $TFN_{2:1}$-CNT membranes declined from 70% to 50%, which demonstrated that the PA layer of $TFN_{2:1}$ and $TFN_{2:1}$-CNT was much loosener than $TFN_{4:1}$ and $TFN_{4:1}$-CNT membranes. It was speculated that DOTAP provided more positive charge and it was more easily to form hydrogen bond between liposomes and not only amine but also benzene ring provided by MPD molecules, therefore limited the diffusion of MPD molecules into reaction zone to react with TMC and formed a relative loosen PA layer[36,37]. Structure and surface function group changes of the PA layer was believed to be benefit the water permeation.

Table 2. Surface elemental composition of TFN membranes.

Membrane	Surface elemental composition					
	C (%)	N (%)	O (%)	P (%)	$R_{O/N}$	D (%)
$TFN_{4:1}$	76.35	10.63	12.59	0.43	1.18	74.7
$TFN_{4:1}$-CNT	74.22	11.73	13.66	0.38	1.16	77.2
$TFN_{2:1}$	71.84	11.82	15.95	0.39	1.35	55.4
$TFN_{2:1}$-CNT	74.81	10.74	16.3	0.15	1.33	57.3

3.3. Surface morphology and roughness of TFC and TFN membranes

Figures 3 and S4 showed the surface morphology of TFN and TFC membranes. Rather than the traditional "ridge-and-valley" structure of TFC membranes, TFN membranes presented "leaf-like" structure due to the incorporation of liposomes and CNT-liposomes in the selective layer, and higher loading concentration induced larger "leaf-like" structure[7,16]. It has been reported that hydrophilic nanoparticles could enhance the miscibility of organic and aqueous phases, thus expanding the IP reaction zone and interfering the chemical reaction between MPD and TMC[38]. It should be mentioned that for $TFN_{2:1}$ and $TFN_{2:1}$-CNT membranes, slight difference can be found compared to $TFN_{4:1}$ and $TFN_{4:1}$-CNT membranes. Specially, under same loading concentration of liposomes or CNT-liposomes, $TFN_{2:1}$ and $TFN_{2:1}$-CNT membranes seemed to present larger "leaf-like" structure on the membrane surface. Besides, rougher surface for $TFN_{2:1}$-CNT membranes can be observed from the cross-section image in Figure 4. It was speculated that the initial formed PA layer limited amine monomer permeant into the reaction region to react with TMC molecules due to the lower diffusion of amine monomer as discussed above, therefore ununiform and larger 'leaf-like' structure occurred on the membrane surface[19]. Of note, insertion of CNT in the liposomes induced obvious aggregation under higher loading concentration (1.0 mg/mL), and $TFN_{2:1}$-CNT membranes exhibited the most serious aggregation among the four different TFN membranes, which was likely caused by the nano-effect of CNT since $TFN_{2:1}$-CNT membrane possessed more quantity of inserted CNT in the liposomes. Table 3 summarized the surface roughness of TFC and TFN membranes under 0.6 mg/mL loading concentration of liposomes and CNT-liposomes, and the relevant AFM images were displayed in Figure S5. It can be clearly found that all the TFN membranes exhibited higher roughness than TFC membranes, which was resulted from the large "leaf-like" structure. Besides, $TFN_{2:1}$-CNT-0.6 membranes exhibited the roughest surface, which was in accordance with the observation from the cross-section images. As discussed above, positively charged DOTAP brought more quantity of inserted CNT in the liposomes and higher surface roughness of the TFN membranes, which was no doubt to be benefit for the membrane permeability.

Preprints (www.preprints.org) | NOT PEER-REVIEWED | Posted: 3 January 2024 doi:10.20944/preprints202401.0120.v1

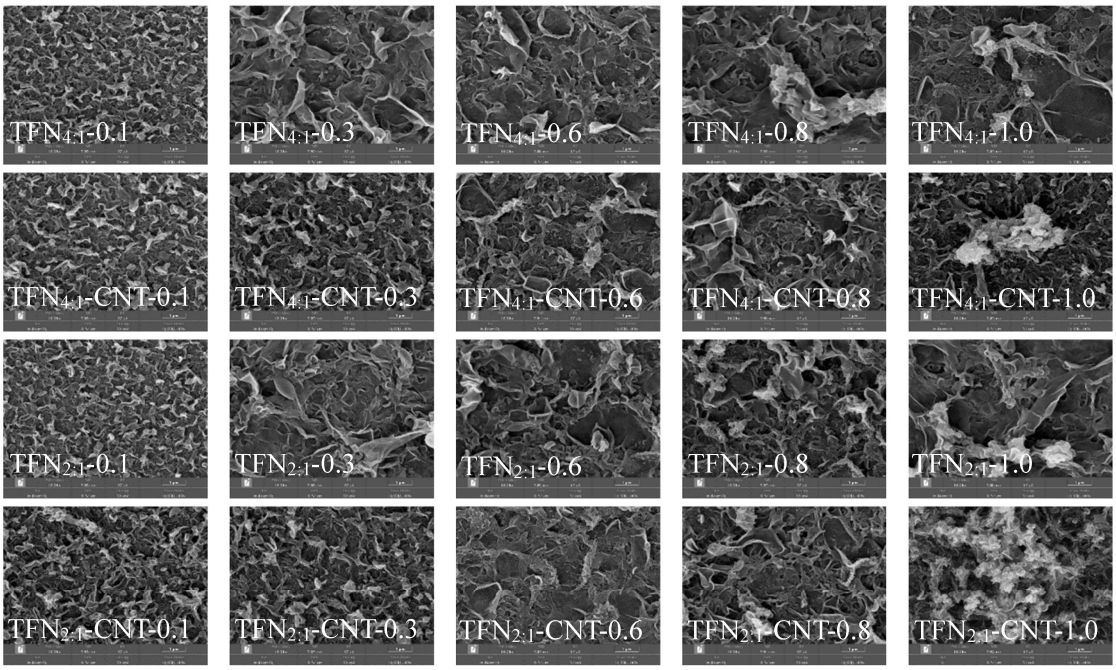

Figure 3. Surface morphology of TFN membranes under different loading concentration of liposomes.

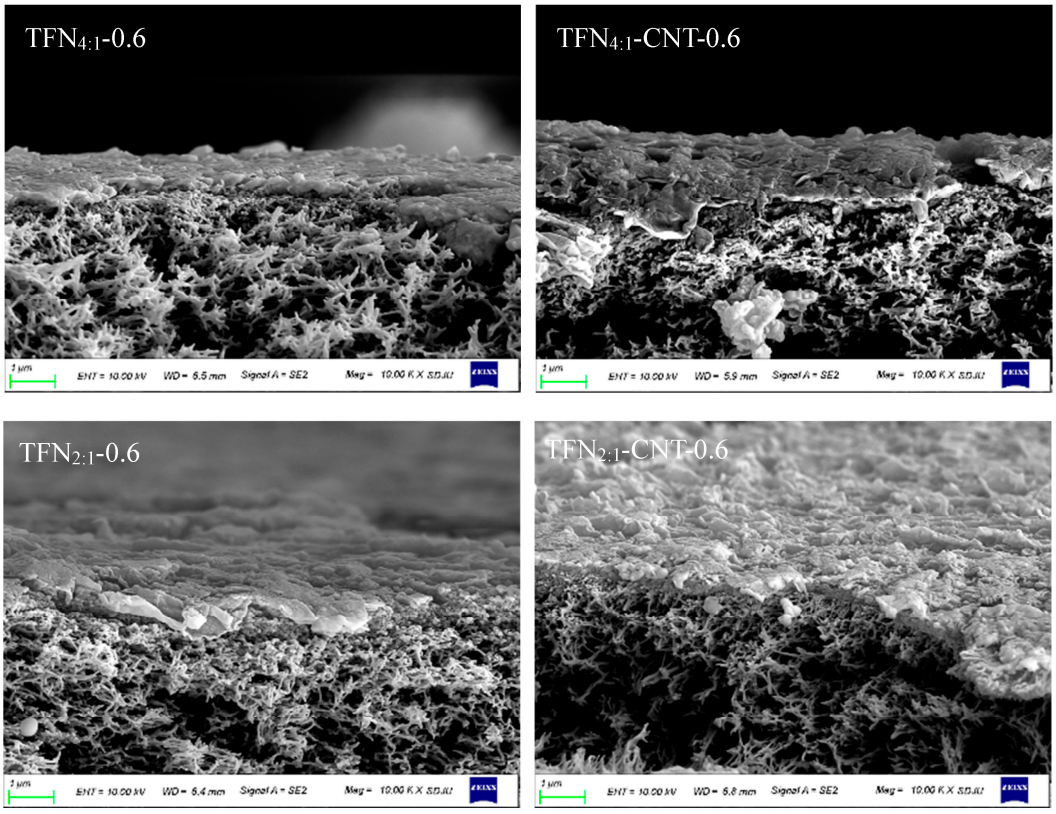

Figure 4. Cross-section images of TFN membranes under 0.6 mg/mL loading concentration of liposomes and CNT-liposomes.

Preprints (www.preprints.org) | NOT PEER-REVIEWED | Posted: 3 January 2024 doi:10.20944/preprints202401.0120.v1

Table 3. Surface roughness of TFC and TFN membranes.

Membrane	Roughness parameters		
	Ra (nm)	Rq (nm)	Rmax (nm)
TFC	87.4	111	812
$TFN_{4:1}$-0.6	143	177	1129
$TFN_{2:1}$-0.6	145	187	1307
$TFN_{4:1}$-CNT-0.6	151	191	1457
$TFN_{2:1}$-CNT-0.6	158	211	1724

3.4. Membrane potential and surface hydrophilicity of TFC and TFN membranes

Figure 5a displayed the membrane potential of TFC and TFN membranes. Generally, protonation of amine groups leads to positive membrane charge at low pH, while deprotonation of carboxylic acid groups leads to negative charge at high pH[39]. As observed from Figure 5a, all the membranes showed decrease trend of membrane potential from pH=3 to pH=10. The membrane potential of four TFN membranes under 0.6 mg/mL loading concentration followed the order $TFN_{2:1}$-CNT-0.6<$TFN_{2:1}$-0.6<$TFN_{4:1}$-CNT-0.6<$TFN_{4:1}$-0.6, which was mainly related to the surface COOH content as analyzed by XPS. Figure 5b–d reflected the hydrophilicity of $TFN_{4:1}$ membrane, $TFN_{2:1}$ membrane and $TFN_{2:1}$-CNT membrane under different loading concentration. For the PS membrane, the contact angle was 76.3°. After formation of PA layer on the membranes surface, the contact angle decreased from 76.3° to 55.3°, which was originated from the changes of the surface function groups and micro-structure. Incorporation of liposomes or CNT-liposomes induced further decline of contact angle, and the more liposomes or CNT-liposomes incorporated, the smaller contact angle obtained, which suggested that surface hydrophilicity was further improved. For the $TFN_{4:1}$ membrane and $TFN_{2:1}$ membrane, little difference was found in the contact angle. However, insertion of CNT in the liposomes caused relatively obvious decline of contact angle for $TFN_{2:1}$-CNT membranes compared to $TFN_{4:1}$ membrane and $TFN_{2:1}$ membrane. For example, under 0.6 mg/mL loading concentration, the contact angle of $TFN_{2:1}$-CNT membrane was 27.7°, while the contact angle of $TFN_{4:1}$ membrane and $TFN_{2:1}$ membrane was 30.1° and 30.3°. Although the decline degree was small, it would still contribute to the fast spreading of water molecules on the membrane surface[2,6]. Except for the changes of surface functional groups and structure (such as COOH content and surface roughness) for all TFN membranes, the presence of CNT in $TFN_{2:1}$-CNT-0.6 membranes also played a vital role in improving the surface hydrophilicity, since it can provide extra hydrogen bond between CNT and water molecules and further accelerate the spreading of water molecules on the membrane surface[9,40].

Preprints (www.preprints.org) | NOT PEER-REVIEWED | Posted: 3 January 2024 doi:10.20944/preprints202401.0120.v1

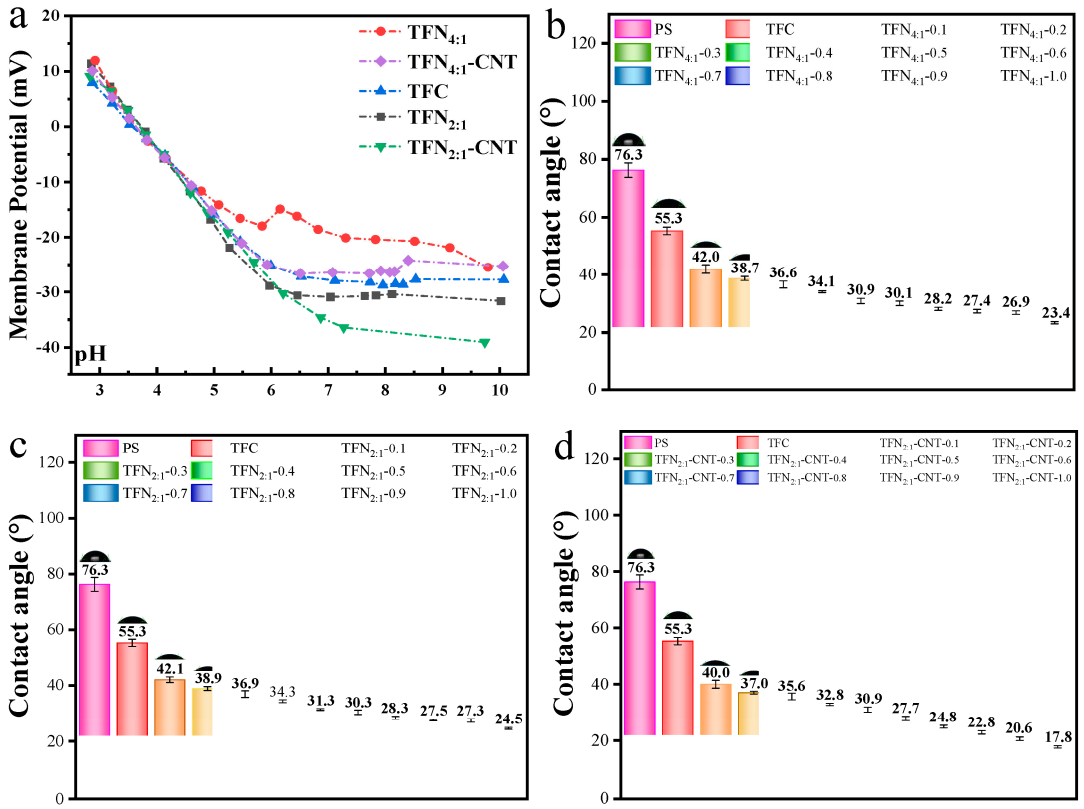

Figure 5. Membrane potential and surface hydrophilicity of TFC and TFN membranes.

3.5. Separation performance of TFC and TFN membranes

Figure 6a displayed the separation performance of TFN membranes, and the change trend of the water flux and salt rejection of TFN membranes under different loading concentration can be found in Figure S6. For TFC membrane, it exhibited 25.2 L/m²·h water flux with 98.6% NaCl rejection and incorporation of liposomes and CNT-liposomes brought remarkable increase in water flux. More important, the salt rejection of TFN membranes maintained almost unchanged compared to TFC membranes, which suggested that liposomes or CNT-liposomes did not destroy the integrity of the PA layer and introduced little defects in the selective layer[41,42]. For $TFN_{4:1}$ and $TFN_{2:1}$ membrane, no obvious difference in water flux, but both of them exhibited 1.67 times higher than TFC membranes. The enhancement of the membrane flux was mainly account for the improved surface properties, such as hydrophilicity and surface roughness, which provided better affinity surface for water molecules to adsorb and further penetrate across the membrane[43]. Moreover, as determined in the *Stop-Flow* test, DOPE/DOTAP liposomes was not thoroughly impermeable for water molecules, therefor it can also serve as the low-resistance water channel and contribute to the increased water permeability. After insertion of CNT in the liposomes, further increment of water flux was detected in TFN-CNT membranes. For $TFN_{4:1}$-CNT membranes, it showed 36.7% increment compared to $TFN_{4:1}$ membrane and 136.5% compared to TFC membranes, which was originated from the fast transformation of water molecules through the inner wall of CNT[44]. For $TFN_{2:1}$-CNT membranes, higher water flux (63.6 L/m²·h) obtained than $TFN_{4:1}$-CNT membranes. As discussed above, the surface hydrophilicity and roughness of $TFN_{4:1}$-CNT and $TFN_{2:1}$-CNT membranes showed nearly no difference, and 1.1 times higher water flux for $TFN_{2:1}$-CNT membrane than $TFN_{4:1}$-CNT membrane was mainly caused by the more quantity of CNT that provided more water channels. Above observation further demonstrated that positively charged DOTAP was of great significance in increasing the quantity of the inserted CNT in the liposomes and then contributing to the better permeability of TFN membranes.

Preprints (www.preprints.org) | NOT PEER-REVIEWED | Posted: 3 January 2024 doi:10.20944/preprints202401.0120.v1

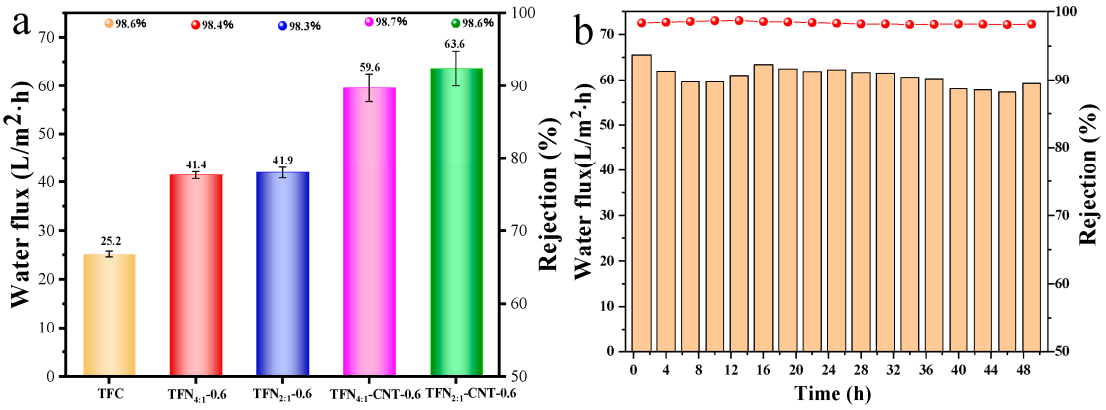

Figure 6. Separation performance of TFC and TFN membranes (a), and stability of $TFN_{2:1}$-CNT-0.6 membranes during 48 h RO test (b).

The stability of long-term RO test was essential for the practical application of TFN membranes. Figure 6b displayed the change trend of water flux and salt rejection of $TFN_{2:1}$-CNT-0.6 membranes during the 48 h RO test. It was satisfied to find that the salt rejection for NaCl maintained unchanged during the long-term RO test, which suggested that $TFN_{2:1}$-CNT-0.6 membrane possessed great stability, not only for the stability of PA layer that could endure the high operation pressure, but also for the stability of CNT-liposomes that could exist stably in the PA layer. The water flux of TFN membranes exhibited slight fluctuant during the long-term RO test. At the first 9 h, the water flux present obvious decline, which was mainly caused by the concentration polarization occurred on the membrane surface that weakened the effective transmembrane pressure[45]. Then the water flux gradually went up and stayed relative stable until the RO test ended up. The excellent stability of the current TFN membranes can be attributed to the great compatibility between CNT-liposomes and PA layer. Besides, liposomes provided extra active amine that could also react with TMC molecules, thereby further enhanced its stability in the PA layer.

3.6. Antifouling performance of TFC and TFN membranes

Figure 7 showed the change trend of water flux and flux recovery rate of TFC and TFN membranes during the fouling test. As seen in Figure 7a, compared to the sharp decline of water flux for TFC membranes, both TFN and TFN-CNT membranes exhibited a relative slower decrease trend and lower pollution level in cycle 1 and cycle 2, which was due to the improved surface properties. The final flux recovery rates (*FRR*) were 72.7%, 85.7%, 87.5%, 90.2% and 91.0% for TFC and TFN membranes, respectively. Of note, $TFN_{2:1}$-CNT-0.6 membranes presented the best antifouling capacity, which was believed to be devoted to the best hydrophilicity and lowest surface negative charge that reduced the absorption capacity of the organic foulant molecules and led to a loosen boundary layer than that on the TFC membrane[46]. Table 3 summarized four antifouling parameters (R_t, R_m, R_r *and* R_{ir}) of TFC and TFN membranes. For TFC membranes, it suffered the most severe membrane fouling with the total resistances of 3.52×10^{13} m^{-1}. The irreversible fouling occupied the dominated position with the resistance about 9.60×10^{12} m^{-1}, which was mainly caused by the pore blocking and formation of dense boundary layer that was hardly removed by the simple hydraulic backwash, thus inducing the severe flux decline and low flux recovery rate[47]. On the contrary, $TFN_{2:1}$-CNT-0.6 membrane showed obvious decline in fouling resistance. More important, the irreversible fouling occurred on the membrane surface gradually changed into reversible fouling. Specially, the irreversible fouling resistance decreased from 9.60×10^{12} m^{-1} to 1.07×10^{12} m^{-1}, which the reversible fouling resistance increased from 6.07×10^{12} m^{-1} to 6.94×10^{12} m^{-1}. In other words, the foulants on the membrane were more easily flushed away through physical clean method, which contributed to the highest *FRR*. Best antifouling capacity of $TFN_{2:1}$-CNT-0.6 membrane was attributed to the improved surface properties, such as surface hydrophilicity and surface charge. Besides, more quantity of CNT in the liposomes was also an important factor in enhancing the antifouling

Preprints (www.preprints.org) | NOT PEER-REVIEWED | Posted: 3 January 2024 doi:10.20944/preprints202401.0120.v1

performance. Since the CNT provided extra exclusion to HA molecules, and the inner wall was not easily blocked by HA, therefore it could always supply the water channel after physical cleaning and the more the better, which was benefit for the recovery of the water flux.

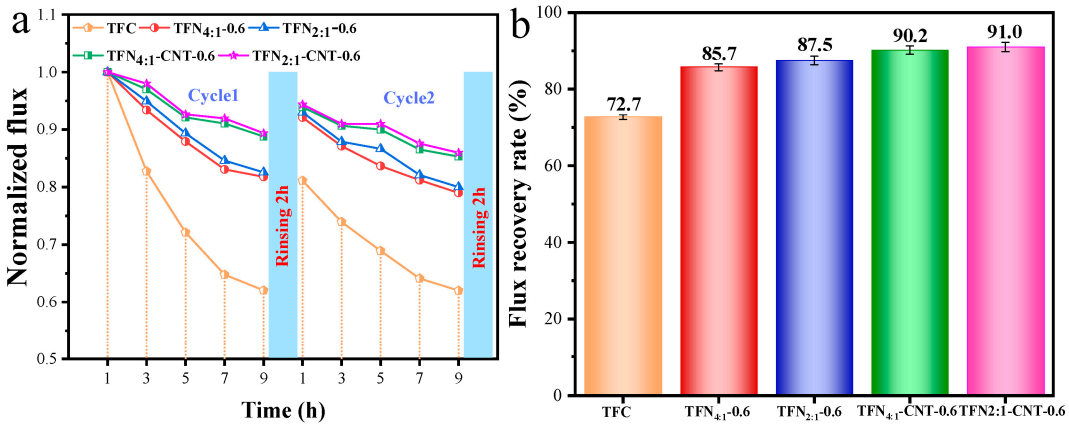

Figure 7. Decline of water flux under antifouling test (a), FRR of TFC and TFN membranes (b).

Table 4. Antifouling parameters of TFC and TFN membranes.

Membrane	R_t (×10^{13} m^{-1})	R_m (×10^{13} m^{-1})	R_r (×10^{12} m^{-1})	R_{ir} (×10^{12} m^{-1})
TFC	3.52	2.56	6.07	9.60
TFN$_{4:1}$-0.6	1.46	1.25	1.24	2.09
TFN$_{2:1}$-0.6	1.39	1.22	1.30	1.74
TFN$_{4:1}$-CNT-0.6	1.12	1.01	6.46	1.10
TFN$_{2:1}$-CNT-0.6	1.19	1.08	6.94	1.07

4. Conclusions

In present study, four types of liposomes (DOPE/DOTAP$_{4:1}$, DOPE/DOTAP$_{2:1}$ DOPE/DOTAP$_{4:1}$-CNT and DOPE/DOTAP$_{2:1}$-CNT liposomes) were synthesized and then incorporated in the selective layer to fabricate TFN membranes. Stop-flow results showed that higher content of DOTAP in the liposome vesicles (DOPE/DOTAP$_{2:1}$-CNT liposomes) induced higher permeability than the liposome vesicles containing lower content of DOTAP (DOPE/DOTAP$_{4:1}$-CNT liposomes), which was resulted from the more quantity of inserted CNT in the liposome vesicles. Addition of DOPE/DOTAP$_{2:1}$-CNT liposomes in the PA layer brought the lowest contact angle, surface charge and highest surface roughness of TFN membranes, which contributed to the best separation performance. 152% flux enhancement than TFC membranes and further 7% flux enhancement than TFN membranes containing DOPE/DOTAP$_{4:1}$-CNT liposomes were obtained. Besides, addition of DOPE/DOTAP$_{2:1}$-CNT liposomes in the PA layer led to 91.0% flux recovery rate with the highest reversible fouling resistance (6.94×10^{12} m^{-1}) and lowest irreversible fouling resistance (1.07×10^{12} m^{-1}). In a word, the present work demonstrated that positively charged DOTAP possesses great potential in increasing the quantity of the CNT inserted in the liposome vesicles, and thus contributing to the better separation and antifouling performance of TFN membranes.

Supplementary Materials: The following supporting information can be downloaded at the website of this paper posted on Preprints.org, Supplementary material including (Materials and chemicals, Preparation of liposomes and CNT-liposomes, Characterization of liposomes and membranes, Experimental setup of RO, TEM images of liposomes, Stopped-flow light scattering curves and osmotic water permeability of liposomes, Surface morphology of TFC membranes, AFM images of TFC and TFN membranes, Water flux and salt rejection of four TFN membranes).

Author Contributions: Jianjun Zhao: Methodology, Formal analysis, Investigation, Data curation, Writing-original draft. Junqing Sun: Formal analysis, Investigation, Data curation. Kefeng Zhang: Investigation, Writing

- review & editing. Shan Wang: Formal analysis, Investigation. Wande Ding: Conceptualization, Writing - review & editing, Funding acquisition, Supervision. Zhengping Li: Software, Formal analysis.

Acknowledgments: This research was supported by the Natural Science Foundation of Shandong Province (ZR2020QB066 and ZR2022QE190) and China Postdoctoral Science Foundation (2020M672122).

Declaration of Competing Interest: The authors declare that they have no known competing financial interests or personal relationships that could have appeared to influence the work reported in this paper.

References

1. Thakur, A.K.; Sathyamurthy, R.; Velraj, R.; Saidur, R.; Lynch, I.; Venkatesh, R.; Kumar, P.G.; Kim, S.C.; Sillanpa, M. A novel solar absorber using activated carbon nanoparticles synthesized from bio-waste for the performance improvement of solar desalination unit. *Desalination* **2022**, *527*, 115564.
2. Li, R.H.; Li, Y.; Wu, H.; Yan, W.T.; Yu, C.Y.; Liu, L.F.; Gao, C.J. Structure regulation for synergistically improving the permeation properties of the reverse osmosis membrane based on an amphiphilic hyperbranched polymer. *J. Membrane Sci.* **2020**, *608*, 118143.
3. Liu, Y.; Wang, X.P.; Zong, Z.A.; Lin, R.J.; Zhang, X.Y.; Chen, F.S.; Ding, W.D.; Zhang, L.L.; Meng, X.M.; Hou, J.W. Thin film nanocomposite membrane incorporated with 2D-MOF nanosheets for highly efficient reverse osmosis desalination. *J. Membrane Sci.* **2022**, *653*, 120520.
4. Zhang, Y.; Wan, Y.; Pan, G.Y.; Yan, H.; Yao, X.R.; Shi, H.W.; Tang, Y.J.; Wei, X.R.; Liu, Y.Q. Surface modification of polyamide reverse osmosis membrane with organic-inorganic hybrid material for antifouling. *Appl. Surf. Sci.* **2018**, *433*, 139-148.
5. Zhao, D.L.; Japip, S.; Zhang, Y.; Weber, M.; Maletzko, C.; Chung, T.S. Emerging thin-film nanocomposite (TFN) membranes for reverse osmosis: A review. *Water Res.* **2020**, *173*, 115557.
6. Yu, C.J.; Cen, X.X.; Ao, D.; Qiao, Z.H.; Zhong, C.L. Preparation of thin-film composite membranes with ultrahigh MOFs loading through polymer-template MOFs induction secondary interfacial polymerization. *Appl. Surf. Sci.* **2023**, *614*, 156186.
7. Yang, L.; Zhang, Q.W.; Wang, Q.K.; Ding, W.D.; Zhang, K.F. Organo-Functionalization: An Effective Method in Enhancing the Separation and Antifouling Performance of Thin-Film Nanocomposite Membranes by Improving the Uniform Dispersion of Palygorskite Nanoparticles. *Membranes-Basel* **2021**, *11*, 889.
8. Jeong, B.H.; Hoek, E.M.V.; Yan, Y.S.; Subramani, A.; Huang, X.F.; Hurwitz, G.; Ghosh, A.K.; Jawor, A. Interfacial polymerization of thin film nanocomposites: A new concept for reverse osmosis membranes. *J. Membrane Sci.* **2007**, *294*, 1-7.
9. Saleem, H.; Zaidi, S.J. Nanoparticles in reverse osmosis membranes for desalination: A state of the art review. *Desalination* **2020**, *475*, 114171.
10. Yang, D.C.; Castellano, R.J.; Silvy, R.P.; Lageshetty, S.K.; Praino, R.F.; Fornasiero, F.; Shan, J.W. Fast Water Transport through Subnanometer Diameter Vertically Aligned Carbon Nanotube Membranes. *Nano Lett.* **2023**, *23*, 4956-4964.
11. Chan, W.F.; Chen, H.Y.; Surapathi, A.; Taylor, M.G.; Shao, X.H.; Marand, E.; Johnson, J.K. Zwitterion Functionalized Carbon Nanotube/Polyamide Nanocomposite Membranes for Water Desalination. *Acs Nano* **2013**, *7*, 5308-5319.
12. Zheng, J.F.; Li, M.; Yu, K.; Hu, J.H.; Zhang, X.; Wang, L.J. Sulfonated multiwall carbon nanotubes assisted thin-film nanocomposite membrane with enhanced water flux and anti-fouling property. *J. Membrane Sci.* **2017**, *524*, 344-353.
13. Khalid, A.; Al-Juhani, A.A.; Al-Hamouz, O.C.; Laoui, T.; Khan, Z.; Atieh, M.A. Preparation and properties of nanocomposite polysulfone/multi-walled carbon nanotubes membranes for desalination. *Desalination* **2015**, *367*, 134-144.
14. Chan, W.F.; Marand, E.; Martin, S.M. Novel zwitterion functionalized carbon nanotube nanocomposite membranes for improved RO performance and surface anti-biofouling resistance. *J. Membrane Sci.* **2016**, *509*, 125-137.
15. Takeuchi, K.; Takizawa, Y.; Kitazawa, H.; Fujii, M.; Hosaka, K.; Ortiz-Medina, J.; Morelos-Gomez, A.; Cruz-Silva, R.; Fujishige, M.; Akuzawa, N.; et al. Salt rejection behavior of carbon nanotube-polyamide nanocomposite reverse osmosis membranes in several salt solutions. *Desalination* **2018**, *443*, 165-171.
16. Wang, Q.K.; Sun, J.Q.; Xue, W.J.; Zhao, G.L.; Ding, W.D.; Zhang, K.F.; Wang, S.; Li, Y.W. Effect of carbon nanotube nanochannel on the separation performance of thin-film nanocomposite (TFN) membranes. *Desalination* **2023**, *546*, 116216.
17. Ding, W.D.; Cai, J.; Yu, Z.Y.; Wang, Q.H.; Xu, Z.N.; Wang, Z.N.; Gao, C.J. Fabrication of an aquaporin-based forward osmosis membrane through covalent bonding of a lipid bilayer to a microporous support. *J. Mater. Chem. A* **2015**, *3*, 20118-20126.

18. Wang, M.Q.; Wang, Z.N.; Wang, X.D.; Wang, S.Z.; Ding, W.D.; Gao, C.J. Layer-by-Layer Assembly of Aquaporin Z-Incorporated Biomimetic Membranes for Water Purification. *Environ. Sci. Technol.* **2015**, *49*, 3761-3768.
19. Sun, J.Q.; Zhang, Q.W.; Xue, W.J.; Ding, W.D.; Zhang, K.F.; Wang, S. An economical and simple method for preparing highly permeable and chlorine-resistant reverse osmosis membranes with potential commercial applications. *Rsc Adv.* **2023**, *13*, 32083-32096.
20. Ding, W.D.; Zhuo, H.W.; Bao, M.T.; Li, Y.M.; Lu, J.R. Fabrication of organic-inorganic nanofiltration membrane using ordered stacking SiO_2 thin film as rejection layer assisted with layer-by-layer method. *Chem. Eng. J.* **2017**, *330*, 337-344.
21. Divya, K.P.; Dharuman, V. Supported binary liposome vesicle-gold nanoparticle for enhanced label free DNA and protein sensing. *Biosens Bioelectron* **2017**, *95*, 168-173.
22. Vaidya, B.; Nayak, M.K.; Dash, D.; Agrawal, G.P.; Vyas, S.P. Development and characterization of site specific target sensitive liposomes for the delivery of thrombolytic agents. *Int. J. Pharmaceut.* **2011**, *403*, 254-261.
23. Martinez-Rubi, Y.; Gonzalez-Dominguez, J.M.; Ansón-Casaos, A.; Kingston, C.T.; Daroszewska, M.; Barnes, M.; Hubert, P.; Cattin, C.; Martinez, M.T.; Simard, B. Tailored SWCNT functionalization optimized for compatibility with epoxy matrices. *Nanotechnology* **2012**, *23*, 285701.
24. Tokgöz, S.R.; Kara, A.; Peksoz, A. Synthesis and characterization of poly(EGDMA--VPCA)/SWCNT composite films by surface polymerization method. *Mat. Sci. Semicon. Proc.* **2020**, *116*, 105144.
25. Song, X.J.; Wang, L.; Tang, C.Y.; Wang, Z.N.; Gao, C.J. Fabrication of carbon nanotubes incorporated double-skinned thin film nanocomposite membranes for enhanced separation performance and antifouling capability in forward osmosis process. *Desalination* **2015**, *369*, 1-9.
26. Tunuguntla, R.H.; Chen, X.; Belliveau, A.; Allen, F.I.; Noy, A. High-Yield Synthesis and Optical Properties of Carbon Nanotube Porins. *J. Phys. Chem. C* **2017**, *121*, 3117-3125.
27. Sanborn, J.R.; Chen, X.; Yao, Y.C.; Hammons, J.A.; Tunuguntla, R.H.; Zhang, Y.L.; Newcomb, C.C.; Soltis, J.A.; De Yoreo, J.J.; Van Buuren, A.; et al. Carbon Nanotube Porins in Amphiphilic Block Copolymers as Fully Synthetic Mimics of Biological Membranes. *Adv. Mater.* **2018**, *30*, 1803355.
28. Genova, J.; Chamati, H.; Petrov, M. Study of SOPC with embedded pristine and amide-functionalized single wall carbon nanotubes by DSC and FTIR spectroscopy. *Colloid Surface A* **2020**, *603*, 125261.
29. Porter, C.J.; Werber, J.R.; Zhong, M.J.; Wilson, C.J.; Elimelech, M. Pathways and Challenges for Biomimetic Desalination Membranes with Sub-Nanometer Channels. *Acs Nano* **2020**, *14*, 10894-10916.
30. Ding, W.D.; Li, Y.M.; Bao, M.T.; Zhang, J.R.; Zhang, C.C.; Lu, J.R. Highly permeable and stable forward osmosis (FO) membrane based on the incorporation of Al_2O_3 nanoparticles into both substrate and polyamide active layer. *Rsc Adv.* **2017**, *7*, 40311-40320.
31. Yin, J.; Yang, Y.; Hu, Z.Q.; Deng, B.L. Attachment of silver nanoparticles (AgNPs) onto thin-film composite (TFC) membranes through covalent bonding to reduce membrane biofouling. *J. Membrane Sci.* **2013**, *441*, 73-82.
32. Fajardo-Diaz, J.L.; Takeuchi, K.; Morelos-Gomez, A.; Cruz-Silva, R.; Yamanaka, A.; Tejima, S.; Izu, K.; Saito, S.; Ito, I.; Maeda, J.; et al. Enhancing boron rejection in low-pressure reverse osmosis systems using a cellulose fiber-carbon nanotube nanocomposite polyamide membrane: A study on chemical structure and surface morphology. *J. Membrane Sci.* **2023**, *679*, 121691.
33. Wang, Z.N.; Wang, X.D.; Ding, W.D.; Wang, M.Q.; Qi, X.; Gao, C.J. Impact of monoolein on aquaporin1-based supported lipid bilayer membranes. *Sci. Technol. Adv. Mat.* **2015**, *16*, 045005.
34. Tayefeh, A.; Poursalehi, R.; Wiesner, M.; Mousavi, S.A. XPS study of size effects of Fe_3O_4 nanoparticles on crosslinking degree of magnetic TFN membrane. *Polymer Testing* **2019**, *73*, 232-241.
35. Shan, M.; Kang, H.; Xu, Z.; Li, N.; Jing, M.; Hu, Y.; Teng, K.; Qian, X.; Shi, J.; Liu, L. Decreased cross-linking in interfacial polymerization and heteromorphic support between nanoparticles: Towards high-water and low-solute flux of hybrid forward osmosis membrane. *J. Colloid Interf. Sci.* **2019**, *548*, 170-183.
36. Yang, Y.; Li, Y.; Goh, K.; Tan, C.H.; Wang, R. Liposomes-assisted fabrication of high performance thin film composite nanofiltration membrane. *J. Membrane Sci.* **2021**, *620*, 118833.
37. Liu, J.W. Interfacing Zwitterionic Liposomes with Inorganic Nanomaterials: Surface Forces, Membrane Integrity, and Applications. *Langmuir* **2016**, *32*, 4393-4404.
38. Baroña, G.N.B.; Lim, J.; Choi, M.; Jung, B. Interfacial polymerization of polyamide-aluminosilicate SWNT nanocomposite membranes for reverse osmosis. *Desalination* **2013**, *325*, 138-147.
39. Asempour, F.; Akbari, S.; Bai, D.; Emadzadeh, D.; Matsuura, T.; Kruczek, B. Improvement of stability and performance of functionalized halloysite nano tubes-based thin film nanocomposite membranes. *J. Membrane Sci.* **2018**, *563*, 470-480.
40. Goh, P.S.; Ismail, A.F. A review on inorganic membranes for desalination and wastewater treatment. *Desalination* **2018**, *434*, 60-80.
41. Zhao, D.L.; Japip, S.; Zhang, Y.; Weber, M.; Maletzko, C.; Chung, T.-S. Emerging thin-film nanocomposite (TFN) membranes for reverse osmosis: A review. *Water Res.* **2020**, *173*, 115557.

42. Li, K.; Lee, B.; Kim, Y. High performance reverse osmosis membrane with carbon nanotube support layer. *J. Membrane Sci.* **2019**, *592*, 117358.
43. Roy, K.; Mukherjee, A.; Maddela, N.R.; Chakraborty, S.; Shen, B.; Li, M.; Du, D.; Peng, Y.; Lu, F.; García Cruzatty, L.C. Outlook on the bottleneck of carbon nanotube in desalination and membrane-based water treatment—A review. *J. Environ.Chem. Eng.* **2020**, 8, 103572.
44. Ali, S.; Rehman, S.A.U.; Luan, H.-Y.; Farid, M.U.; Huang, H. Challenges and opportunities in functional carbon nanotubes for membrane-based water treatment and desalination. *Sci. Total Environ.* **2019**, *646*, 1126-1139.
45. Lee, K.P.; Arnot, T.C.; Mattia, D. A review of reverse osmosis membrane materials for desalination—Development to date and future potential. *J. Membrane Sci.* **2011**, *370*, 1-22.
46. Zhao, S.; Liao, Z.; Fane, A.; Li, J.; Tang, C.; Zheng, C.; Lin, J.; Kong, L. Engineering antifouling reverse osmosis membranes: A review. *Desalination* **2021**, *499*, 114857.
47. Zhang, T.; Li, Z.; Wang, W.; Wang, Y.; Gao, B.; Wang, Z. Enhanced antifouling and antimicrobial thin film nanocomposite membranes with incorporation of Palygorskite/titanium dioxide hybrid material. *J. Colloid Interf. Sci.* **2019**, *537*, 1-10.